Title: Performance of a single layer fuel cell based on a mixed proton-electron conducting composite

Author names and affiliations: Krzysztof Zagórski[a], Sebastian Wachowski[a], Dagmara Szymczewska[b], Aleksandra Mielewczyk-Gryń[a], Piotr Jasiński[b], Maria Gazda[a]

[a] Faculty of Applied Physics and Mathematics, Gdansk University of Technology, Narutowicza 11/12, 80-233 Gdansk, Poland

[b] Faculty of Electronics Telecommunications and Informatics, Department of Biomedical Engineering, Gdansk University of Technology, Narutowicza, Gdansk, Poland

Corresponding author:

Krzysztof Zagórski
Faculty of Applied Physics and Mathematics
Gdansk University of Technology
Narutowicza 11/12
80-233 Gdansk
Poland
Tel. +48 58 348 66 12
Fax. +48 58 347 28 21
E-mail: kzagorski@mif.pg.gda.pl

Abstract

Many of the challenges in solid oxide fuel cell technology stem from chemical and mechanical incompatibilities between the anode, cathode and electrolyte materials. Numerous attempts have been made to identify compatible materials. Here, these challenges are circumvented by the introduction of a working single layer fuel cell, fabricated from a composite of proton conducting $BaCe_{0.6}Zr_{0.2}Y_{0.2}O_{3-\delta}$ and a mixture of semiconducting oxides – Li_2O, NiO, and ZnO. Structural and electrical properties of the composite, related to its fuel cell performance are investigated. The single layer fuel cell shows a maximum OCV of 0.83 V and a peak power density of 3.86 mW cm^{-2} at 600 °C. Activation and mass transport losses are identified as the major limiting factor for efficiency and power output.

Keywords
Mixed electronic ionic conductor; solid oxide fuel cells; composites; single layer; proton conductor; barium cerate

1. Introduction

Since the 1970s fuel cells have been heralded as one of the foundations of the hydrogen economy – coal and petroleum fuels were to be replaced by hydrogen as the primary source of clean and green energy [1]. After over 40 years this is still not the case, mostly due to the high cost of fuel cells which limits them to niche applications [2–5]. There are three major factors influencing fuel cell costs. Firstly, the use of expensive raw materials, particularly the noble metals used as catalysts (mostly for low-temperature cells). Secondly, low durability and reliability – especially in the case of high-temperature devices [5–8]. Finally, the complexity of manufacturing a state of the art fuel cell, which is usually composed of three distinct functional layers [2]. Each layer is made from a different material with varying chemical and mechanical properties – these variations are the source of the aforementioned incompatibilities and some of the major factors in decreasing fuel cell durability [8–12].

The layered structure is considered strictly necessary – it prevents the short-circuiting of the cell. That preconception was first challenged in 2000 by He et al. [13,14], who reasoned that $La_{1-x}Sr_xInO_3$ – a mixed ion-electron conducting material – could be used as a single layer solid oxide fuel cell due to mixed n-type, oxygen ion or p-type conductivity at different pO_2 values. The $La_{1-x}Sr_xInO_3$ cell was able to generate electromotive force and a maximum power density of 3 mW cm^{-2} was

reported, which proved the viability of the concept, but no further research has been done regarding $La_{1-x}Sr_xInO_3$ single layer fuel cells (SLFCs). Zhu et al. further challenged the triple layer paradigm of fuel cell design in 2011, with a composite of an oxide ion conducting ceramic (samaria doped ceria) and metal oxide semiconductors (Li_2O, NiO, ZnO) exhibiting both electron and hole conductivity. A single layer of the composite can operate as a fuel cell device [15,16]. Zhu et al. hypothesize that in single layer fuel cells at operational conditions a space charge region, similar to the bulk heterojunction in dye-sensitized solar cells, is formed which acts as a block for electron transfer, thereby performing one of the functions of a conventional electrolyte [17]. Mass and charge transport are claimed to be possible, despite the space charge region, thanks to surface diffusion enabled and promoted by high porosity [18]. So far, there have been no reports of experiments validating the proposed mechanism. Understanding of the processes occurring in SLFCs is necessary for the determination of the properties of composite components such as microstructure and porosity that are optimal for the maximization of fuel cell characteristics. For example, the role of porosity is not clear, since apart from providing paths for the surface diffusion it may also cause a direct combustion reaction between oxygen and hydrogen in the bulk of the cell, leading to a rapid cell failure [19].

SFLCs based on composites of various materials have been reported, some with a protonic component [20–26]. In each case, however, oxygen ions were the main charge carriers. High-temperature proton conductors (HTPCs) are considered as a

promising alternative to oxygen ion conductors for the intermediate temperature range of 400–700 °C. State-of-the-art oxygen ion conducting fuel cells operate in the temperature range of 800–1000 °C [27]. Proton conductors, due to the generally higher mobility of their charge carriers, have a lower activation energy of conduction than that of oxygen ion conduction. This lower activation energy of conduction is a major factor contributing to higher conductivity at the intermediate temperatures [28]. Therefore, replacing the oxygen ion conductors in composites for single layer fuel cells with a proton conducting material would lower the working temperatures of SLFCs providing many benefits, such as easier sealing, the better economy of fabrication, rapid startup and a decrease in thermal stresses caused by a mismatch of thermal expansion coefficients [29].

In this paper, we investigate the properties of a composite of co-doped barium cerate, a well-established proton conductor, and a mixture of semiconducting oxides: Li_2O, NiO, and ZnO. We also discuss the composite's performance when applied as a single layer fuel cell material.

2. Experimental

2.1.Synthesis

The $BaCe_{0.6}Zr_{0.2}Y_{0.2}O_{3-\delta}$ (BCZY622) proton conducting nanopowders were prepared by co-precipitation method [16,30]. Stoichiometric amounts of nitrate powders – $Ba(NO_3)_2$, $Ce(NO_3)_3 \cdot 6H_20$, $ZrO(NO_3)_2 \cdot 2H_20$ and $Y(NO_3)_3 \cdot 6H_20$ – were dissolved in deionized water resulting in a 0.5 M solution of metal cations. A 0.5 M

aqueous solution of Na_2CO_3 was used as a precipitation agent. The Na_2CO_3 solution was dripped into the cation solution at a rate of approximately 10 cm^3 min^{-1} under constant stirring and heating. The resulting precipitate was washed thoroughly with deionized water and then dried at 80 °C for 24 hours. The dried powder was calcined at 1100 °C for five hours, subsequently pressed uniaxially and sintered using a two-step approach [30].

The Li_2O:NiO:ZnO (LNZ) semiconducting oxides were prepared by the solid-state synthesis method. Stoichiometric amounts of ZnO, $LiCO_3$, and $Ni(NO_3)_2 \cdot 6H_2O$ powders were mixed to give a cation ratio of 0.15:0.45:0.4, ground in an agate mortar and calcined at 800 °C for 2 hours [16].

The BCZY622 and LNZ precursor powders in the weight ratio of 2:1 were mixed in an agate mortar, and then ball milled in isopropanol for 24 hours [19,20,31]. The resultant BCZY622/LNZ composite powder was dried at 80°C for 24 hours and then pressed uniaxially into pellets 12 mm in diameter and approximately 1 mm thick. The pellets were subsequently sintered using a two-step approach. At first, they were heated to 1200 °C with a 5 °C min^{-1} heating rate, held for 1 minute, cooled with a 15 °C min^{-1} rate to 900 °C and then maintained for 2 hours, resulting in dense pellets with no visible cracks or other faults.

2.2. Characterization

The density and porosity of SLFC pellets were measured using a vacuum-assisted Archimedes method. It was then compared with the composite's theoretical density, calculated as a weighted average of theoretical densities of BCZY622 and LNZ [19].

X-ray diffractometry data on BCZY622, LNZ, and the BCZY622/LNZ composite was collected by a Philips X' Pert Pro diffractometer, with CuKα radiation.

Photomicrographs were captured using an FEI QUANTA FEG 250 scanning electron microscope (SEM) with a secondary and backscattered electron detector. Energy dispersive X-ray analysis was also performed, utilizing an EDAX TEAM™ EDS Analysis System. The composite pellets, both as sintered and after operation in fuel cell conditions, were imaged under high vacuum. Because of their high electronic conductivity, an additional metallic coating was not required.

In preparation for measurements of electrical properties, electrodes made from silver and yttria stabilized zirconia paste were painted on each side of the pellet, which was 10.14 mm in diameter and 1.11 mm thick. Each electrode had a diameter of 9.00 mm which translates into an area of 0.64 cm^2, which was later used for ASR calculations using the general equation $ASR = R \cdot A$, where R is the resistance derived from impedance spectroscopy and A is the electrode area. The composite BCZY622/LNZ pellet was then mounted on a testing cell and sealed with silver paste [32]. The same atmospheres for all electrical property measurements were applied – one side of the pellet was exposed to 5% humidified H_2 with a 30 cm^3 min^{-1} flow rate, the other to flowing air. For open circuit voltage (OCV) and current-voltage characteristic (I-V) measurements, a Solatron SI 1287 Electrochemical Interface was

used. Impedance spectroscopy (IS) measurements were carried out using a Solatron SI 1287 Electrochemical Interface coupled with a Solatron SI 1260 Impedance Analyzer, in the 1 MHz – 0.1 Hz frequency range. The impedance data was analyzed using Equivalent Circuit software [33].

3. Results & Discussion

Diffraction data of the components and the composite powder are presented in Fig. 1. Crystallographic data derived from Rietveld analysis of the obtained diffractograms are collected in Table 1. In the diffractogram of the Li_2O:NiO:ZnO (LNZ) semiconducting oxides XRD reflections of ZnO and NiO can be seen, whereas no reflections of Li_2O are present. The absence of XRD reflections of Li_2O in the diffractogram of the Li_2O:NiO:ZnO (LNZ) is most probably caused by the lithium diffusion into the oxides. The reflections of NiO are higher than those of ZnO, which means that diffusion of Zn^{2+} cations and O^{2-} anions from ZnO occurs during LNZ calcination. According to H. Kedesdy and A. Drukalsky who analyzed the solid state reaction in the NiO-ZnO system in detail, such processes take place above 600 °C [34]. As a result of lithium diffusion into the oxides and zinc diffusion into NiO, the nickel and zinc oxides compositions are rather (Ni, Zn, Li)O and (Zn, Li)O oxides, respectively. Moreover, an increase of the unit cell parameter of cubic NiO may be expected.

Composite component	Material	Space group	Unit cell parameters [Å]	Unit cell volume [Å^3]
Proton conductor (BCYZ622)	$BaCe_{0.6}Zr_{0.2}Y_{0.2}O_{3-x}$	Imma (no. 74)	a = 6,1696(5) b = 8,6907(6) c = 6.267	336.01
Semiconducting phase (LNZ)	(Ni, Zn, Li)O	Fm-3m (no. 225)	a = 4.19958(1)	74.06
	(Zn, Li)O	$P6_3mc$ (no. 86)	a = 3.24855(3) c = 5.2038(1)	47.56

Table 1 Unit cell parameters of the composite components. The R_p parameter of Rietveld refining for BCYZ622 and LNZ phases were 20 and 7.9, respectively.

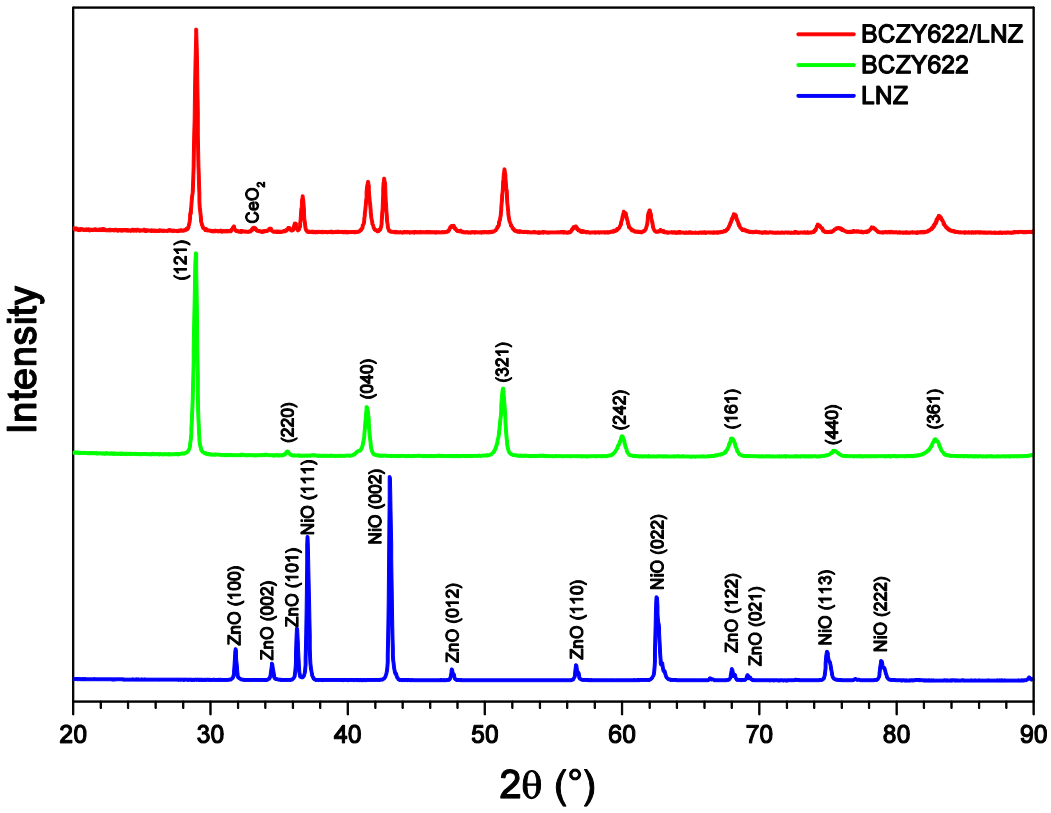

Fig. 1 XRD diffractograms of the $BaCe_{0.6}Zr_{0.2}Y_{0.2}O_{3-\delta}$ (BCZY622), Li_2O:NiO:ZnO (LNZ) and BCZY622/LNZ composite powders.

The unit cell parameter of the cubic (Ni, Zn, Li)O oxide determined with the use of Rietveld analysis (4.1996 Å) is significantly larger than that of the undoped nickel oxide (4.1684 Å). Comparison with the data published in [34] suggests that approximately 18% of Zn is present in the cubic NiO. The unit cell volume and parameters of the hexagonal ZnO do not change significantly as a result of LNZ calcination, so that the Ni diffusion into ZnO may be neglected [35]. As mentioned before, the lithium diffusion into the oxides occurs. The solubility of lithium both in NiO and in ZnO is high, but the nature of the most stable defects formation in both oxides differs. In ZnO, several types of lithium defects, for instance, the interstitial lithium ion, $Li^{\bullet}_{i}$ as well as the $Li^{'}_{Zn}$ - $Li^{\bullet}_{i}$ neutral defect pairs are possible [36]. The most stable one is $Li^{\bullet}_{i}$, which is a donor-type defect since it introduces the energy level below the bottom of the conduction band. On the other hand, in NiO lithium substitutes Ni forming $Li^{'}_{Ni}$, which is an acceptor defect. A weak reflection of cerium oxide can be seen in the diffractogram of the composite BCZY622/LNZ powder. The presence of cerium oxide is caused by barium evaporation, often observed in the case of barium cerates [37].

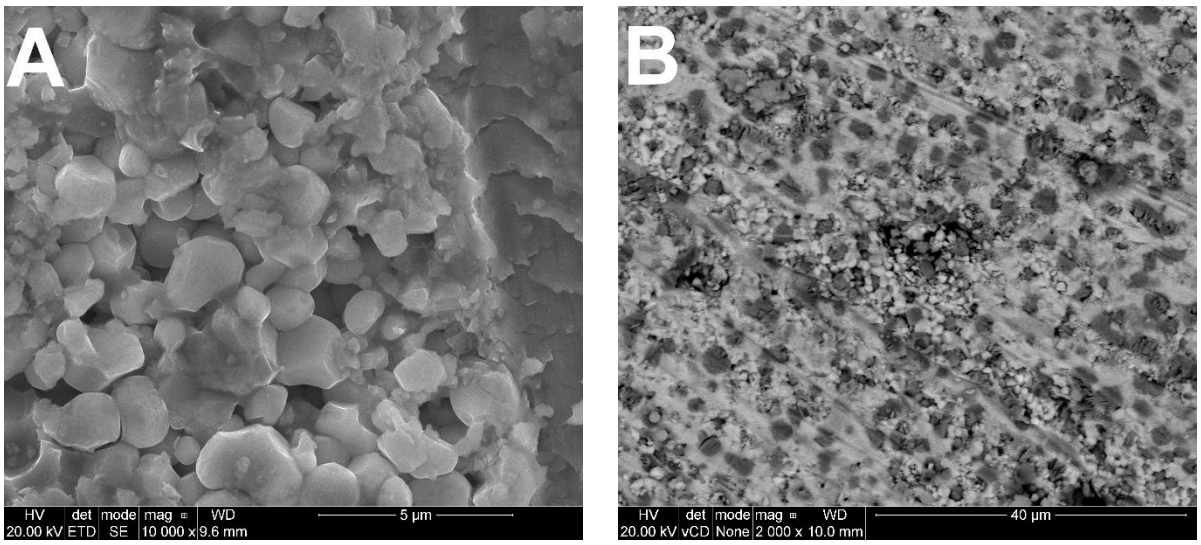

Fig. 2 Cross-sectional SEM photomicrographs of BCZY622/LNZ composite pellets.

Fig. 2 presents cross-sectional SEM photomicrographs of the BCZY622/LNZ composite pellet. Fig. 2A shows the microstructure of the composite. The image in Fig. 2B was taken using a backscattered electron detector (BSED), which allowed phase-contrast imaging – the brighter areas correspond to the proton conducting phase (BCZY622), while the darker areas correspond to the semiconducting oxides (LNZ). It can be seen the LNZ phase is distributed in grains embedded in the BCZY622 matrix. Moreover, only a small amount of pores, which are most likely closed pores, is visible in the material. This agrees well with high material density (>95 % of theoretical density) measured by the Archimedes method [19].

Voltages and power densities as a function of current density, for temperatures between 400 and 600 °C, are plotted in Fig. 3. The highest power density of 3.86 mW cm^{-2} was recorded at 600 °C. Overall, the power densities are low comparing the values reported by Zhu et al. For example, they observed power densities up to 450 mW cm^{-2} in $Ce_{0.9}Gd_{0.1}O_{2-x}$ - $LiNiO_2$ [15], 600 mW cm^{-2} in $Ce_{0.8}Sm_{0.2}O_{2-x}$ -

$LiZnNiO_2$ [16], 655 mW cm^{-2} in $Ce_{0.8}Sm_{0.2}O_{2-x}$ – $Ba_{0.5}Sr_{0.5}Co_{0.8}Fe_{0.2}O_{3-x}$ [38] and 760 mW cm^{-2} in $Ce_{0.8}Sm_{0.2}O_{2-x}$ - $LiCuZnNiO_2$ [17]. Possible reasons for a low power density of the cell based on the $BaCe_{0.6}Zr_{0.2}Y_{0.2}O_{3-x}$ – LNZ composite in comparison to the $Ce_{0.8}Sm_{0.2}O_{2-x}$ – LNZ composite could be sought in either the properties of ion conducting phases or in the composites microstructures. We assume that similarly to conventional oxide fuel cells, both oxygen ion- and proton – conducting oxides are equally appropriate for the functioning of the device provided that they have sufficient conductivities. Ion conductivity values of $Ce_{0.8}Sm_{0.2}O_{2-x}$ and $BaCe_{0.6}Zr_{0.2}Y_{0.2}O_{3-x}$ ceramics at 600 °C are of the order of 10^{-2} S/cm and the activation energies of conductivity are 0.82 eV and 0.78 eV, respectively [38–41]. Therefore, these materials may be considered as comparable in the studied temperature range in the context of SLFC application. On the other hand, the microstructural differences between the composites seem to be significant since the SLFCs reported by Zhu et al. (e.g. [15,16]) were prepared by pressing the powders whereas our cells were compacted by sintering. Indeed, pressing the composite containing nano-ceramic powder may lead to forming a mesoporous but gas-tight and mechanically stable pellet. However, the composite with nano-ceramic barium cerate for achieving long-term stability requires sintering. Therefore, in the future, the microstructure of the composite should be modified to obtain a material containing a larger amount of small pores.

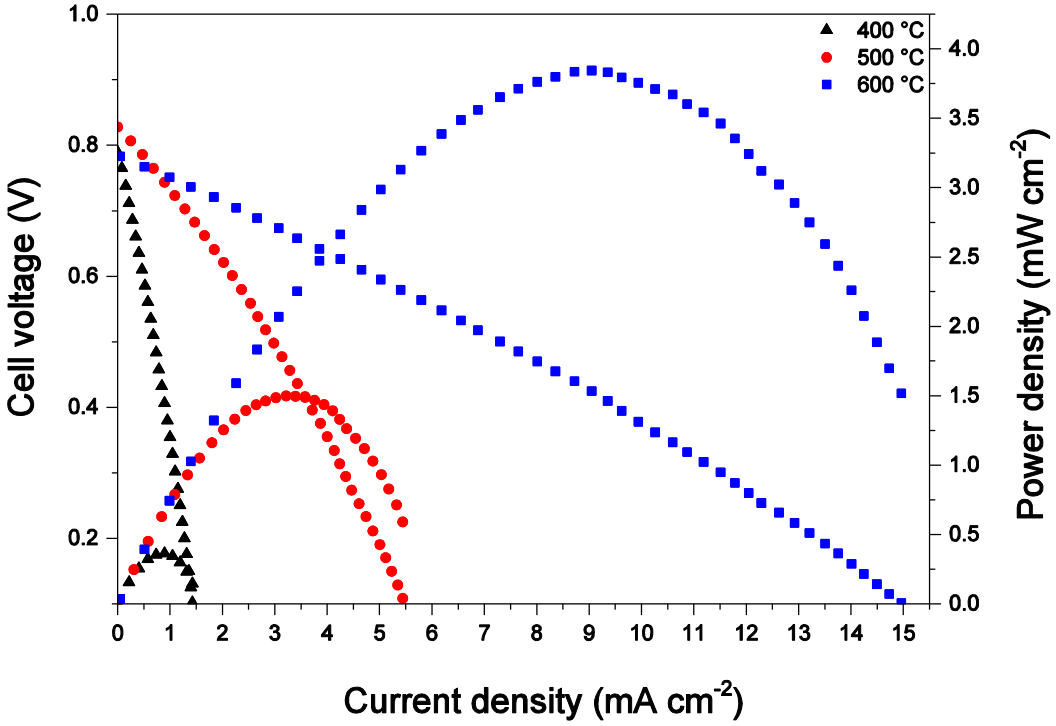

Fig. 3 Cell voltages and power densities measured at temperatures between 400 °C and 600 °C.

An example of the collected impedance spectroscopy spectra of a single layer fuel cell collected at 600 °C and the equivalent circuit used for the fitting are shown in Fig. 4. The fitted spectrum is in good agreement with the collected data. The ohmic and polarization components of area specific resistances (ASRs), derived from the EIS data, are plotted in Fig. 5.

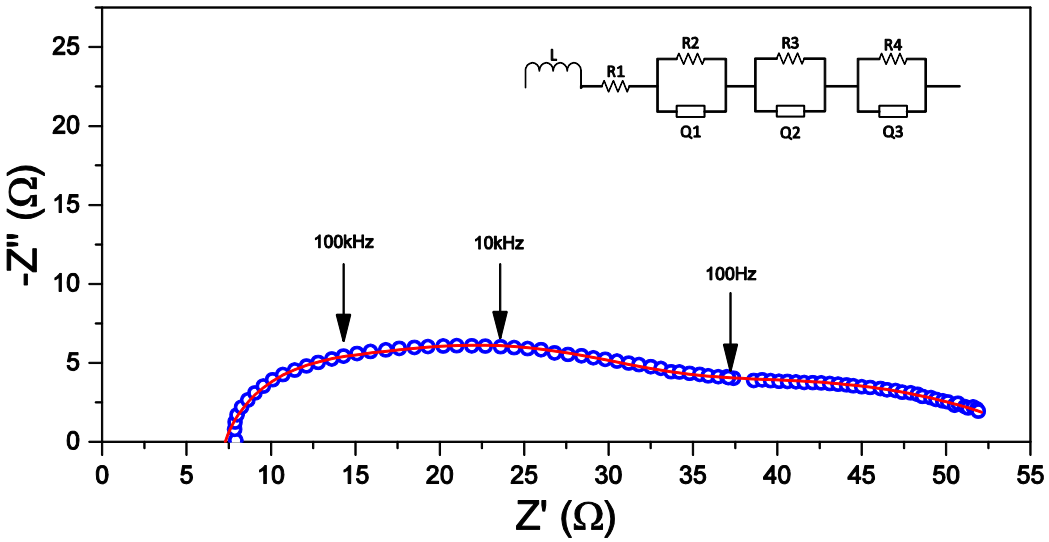

Fig. 4 Example impedance spectrum, measured at 600 °C. The empty circles represent data points, and the line represents the fitting.

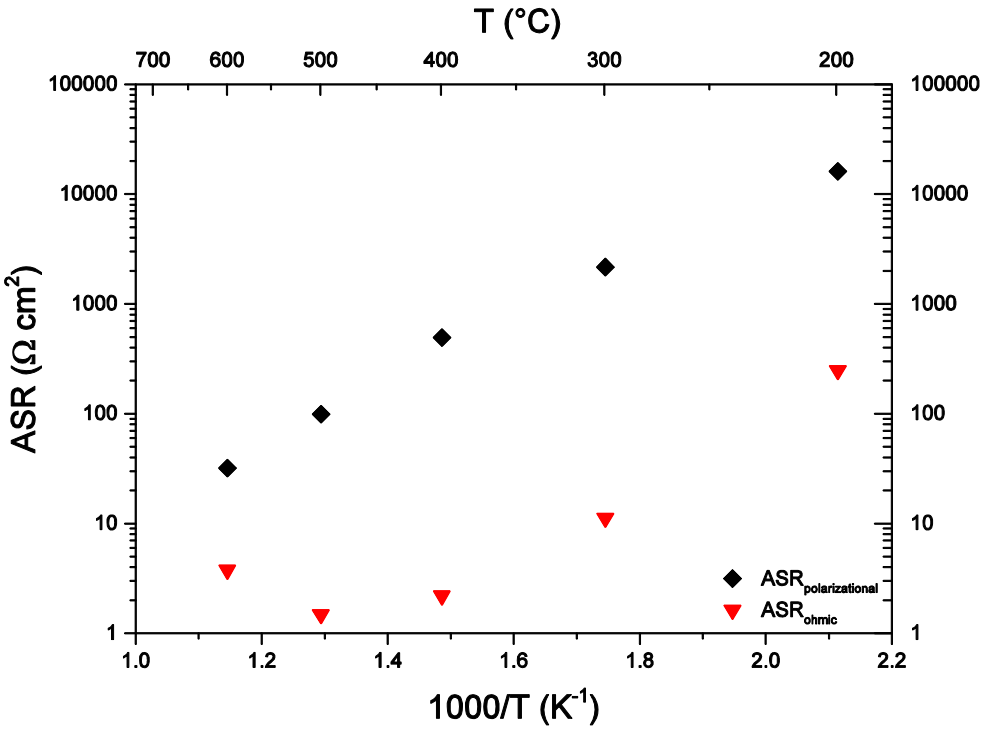

Fig. 5 Ohmic and polarization components of area specific resistance.

The values of the ASR's polarization component are approximately two orders of magnitude higher than that of the ohmic component, which indicates that the major limiting factors for the SLFCs efficiency and power output are activation and mass

transport losses [42]. An ASR value of 0.15 Ω cm^2 is an established target for a commercial thin-film electrolyte SOFC design [43]. The measured values of ASR are orders of magnitude higher and thereby explain the SLFC's low power densities. Possible reasons for high ASR which should be considered include semiconducting junctions amount, space charge layer formation, and too high pellet density. A non-uniform distribution of the semiconducting oxides could lead to an irregular distribution of the p-type (NiO) – n-type (ZnO) heterojunctions formed by neighbouring grains of NiO and ZnO on the nanoscale. Moreover, the formation of (Ni, Zn)O solid solutions, observed in the XRD results, decreases the amount of p (NiO) - n (ZnO) junctions. Maximizing the number of heterojunctions could increase the SLFCs efficiency. In addition to the nanoscale junctions, the space charge layer similar to the bulk heterojunction in dye-sensitized solar cells can also be a contributing factor to the SLFC's impedance and ASR [17,44–46]. Another factor contributing to the low power density and high ASR is high pellet density, which limits charge and mass transport by decreasing the length of the triple phase boundary as well as the active surface area. This is in agreement with the results of SEM/EDS studies. Moreover, it also supports our conclusions from the analysis of the microstructural differences between our cells and these constructed by Zhu et al. As Zhu et al. proposed, the porosity could also be necessary for providing the paths for surface diffusion [18]. On the other hand, our previous studies of a 36% porous system of the same BCZY622/LNZ composite showed a very low open circuit voltage of 0.325 V [19]. Moreover, the stability of the studied cell was also poor; it worked in an oscillatory way and failed after 30 minutes. The low performance of the

porous cell was probably caused by direct combustion of H_2 and O_2 in the bulk of the pellet [19]. What seems most plausible, some porosity of the SLCF material is necessary for the efficient work of the cell, but the size, distribution, and amount of pores should be such that the direct reaction between H_2 and O_2 is not possible. Therefore, a systematic study of the influence of porosity on the SLFC performance is needed. Tailoring the microstructure should help lower the mass transport losses, which would decrease the ASR and increase the power density accordingly. One possible approach would be to create an SLFC with porosity gradients on both sides of the pellet, which would satisfy the demand for porous "functional electrodes" with extended surface areas and a dense and impermeable "functional electrolyte" [47].

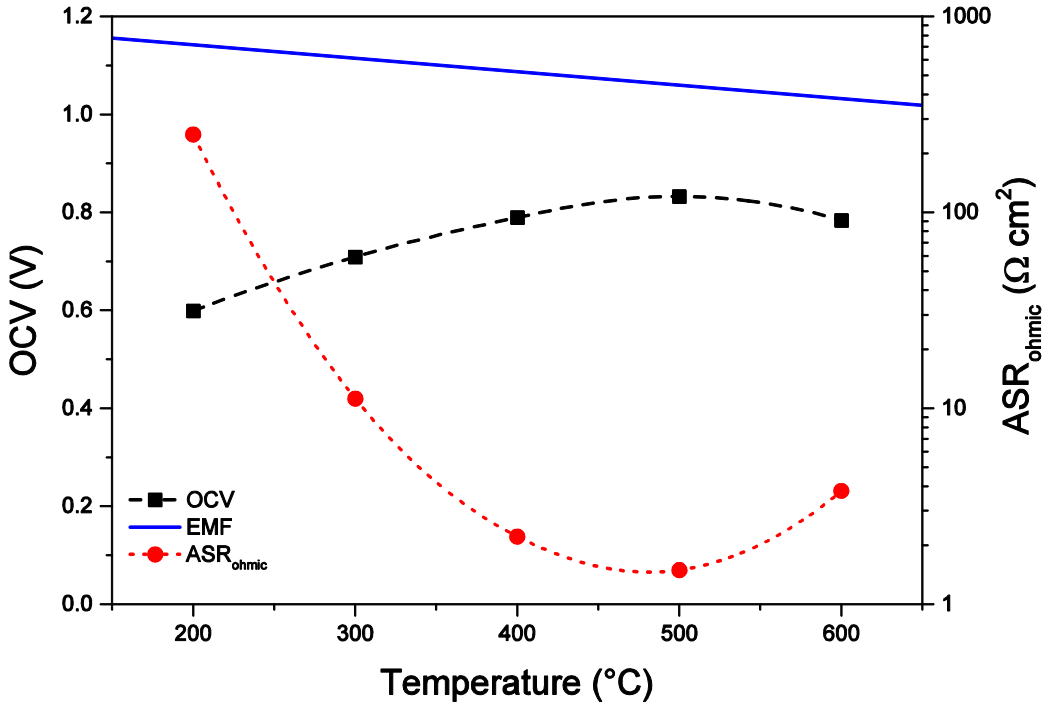

Fig. 6 Open circuit voltage and ASR_{ohmic} as a function of temperature. The solid line represents the theoretical temperature dependence of EMF. The dashed lines are a visual aid only.

The temperature dependence of the open circuit voltage (OCV) is presented in Fig. 6. For comparison, it is plotted together with the ohmic component of the area specific resistance (also presented in Fig. 5) and the electromotive force (EMF), calculated using the Nernst equation [43]. As can be seen, the OCV's temperature dependence is different from that predicted by the Nernst equation. A maximum OCV value of 0.83 V is observed at 500 °C. What is interesting, at a similar temperature a minimum of ohmic area specific resistance is also seen. Assuming that this is not merely a coincidence, this correlation between OCV and ASR temperature dependencies indicates that both are caused by the same reasons. Such a nonmonotonic temperature dependence of OCV and ASR could result from the change of conductivity mechanism with temperature which may be due to to the change of majority charge carrier type at a certain temperature. However, the composite cell was studied at temperatures below 600 °C which means that protons are main charge carriers in barium cerate regardless the oxygen partial pressure [48]. Other probable causes of the nonmonotonic temperature dependence are concurrent and competing processes with different temperature dependencies. Such processes as gas leak, cation diffusion, electron leak, the width of the space charge layer change may jointly influence the conductivity and the electrochemical potential in such a way as to give the observed minimum and maximum, respectively. At the temperature range between 200 and 600 °C, the phenomena related to the diffusion of both lithium and Zn ions in the oxides may be present. In the whole temperature range, especially above 692 K (419 °C), which is quite close to the temperature at which minimum ASR is observed, the processes of ZnO etching and reduction

followed by Zn evaporation (described in more detail below) occur [49]. Moreover, the electron saturation current flowing in semiconducting junctions depends on temperature. This effect, as well as the temperature dependence of the width of the space charge layer, could be considered as weak. Moreover, an increase of the electron saturation current which could cause an electron leak should decrease both OCV and ohmic ASR. Summing up, explanation of the convoluted temperature dependence of OCV and ohmic ASR requires further studies, however, the reactions of hydrogen with ZnO seem most likely to be responsible for this.

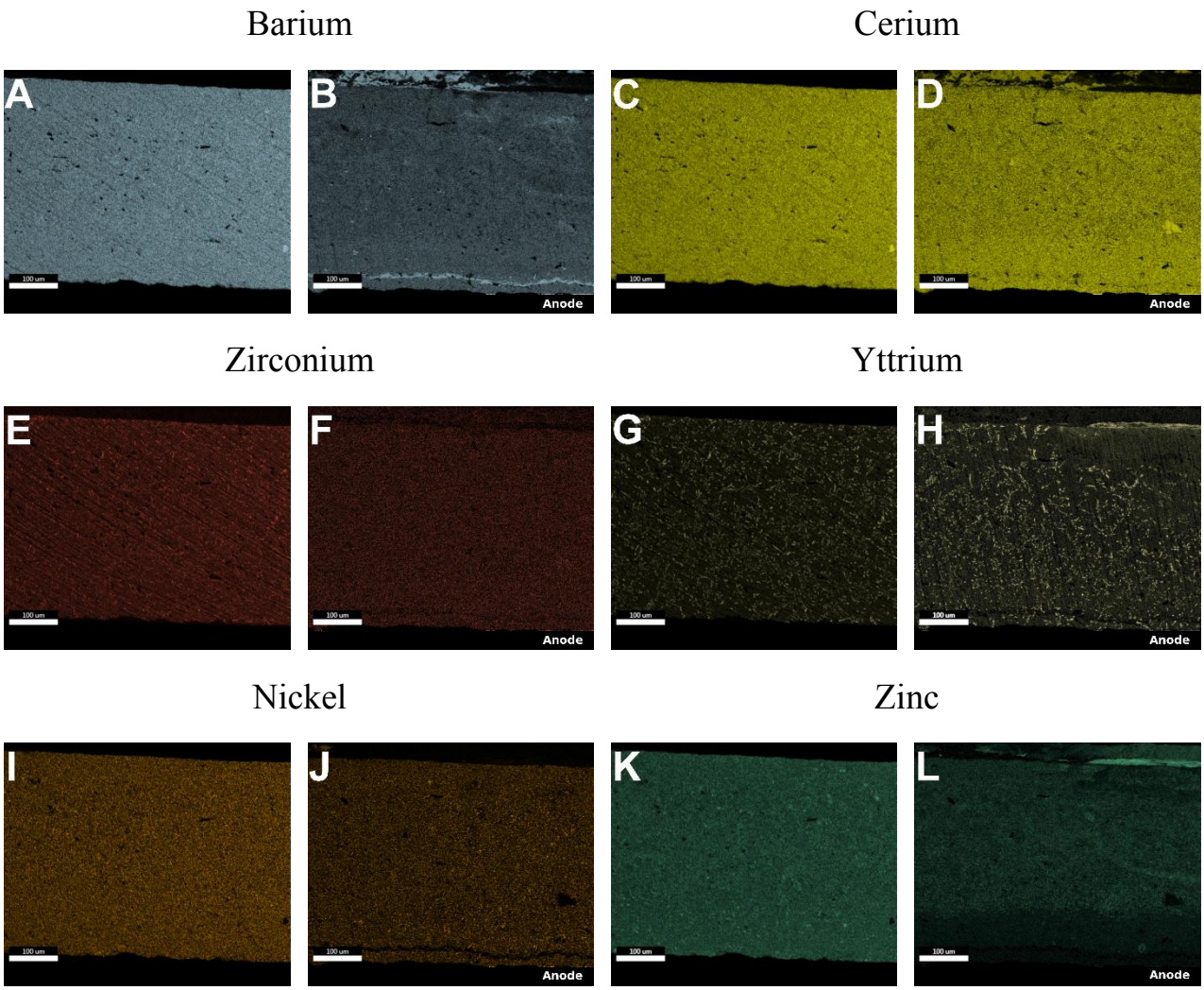

Fig. 7 Cross-sectional EDS maps of element distribution for a BCZY622/LNZ composite pellet. The images annotated "anode" display the pellet that was subjected

to a reducing H_2 atmosphere during long-term OCV measurements. The contrast of the image indicates a higher concentration of the specific element.

EDS maps were collected to examine the influence of the prolonged operation of SLCF's based on the BCZY622/LNZ composite. Fig. 7A – 7L display cross-sectional maps for all elements in the composite, except lithium due to limitations of EDS spectroscopy [50]. Figs.7A, 7C, 7E, 7G, 7I, and 7K show the pellet as synthesized, while Figs. 7B, 7D, 7F, 7H, 7J, and 7L display a pellet that was subjected to a reducing H_2 atmosphere during the long-term OCV measurements. The anode side of that pellet, which was directly exposed to H_2, is located at the bottom of the images. The contrast of the image indicates higher concentration the specific element. As can be seen in the as-synthesized pellet's cross-sectional maps: barium (Fig. 7A), cerium (Fig. 7C), nickel (Fig. 7I) and zinc (Fig. 7K) are evenly distributed throughout the mapped area. Yttrium (Fig. 7G), and to a much lesser extent also zirconium (Fig. 7E), are clearly segregated. The regions rich in Y also seem to be slightly richer in Zr. However, no depletion of either barium or cerium is observed. In the maps of the reduced pellet, two key differences become evident. Firstly, the area with a noticeable abundance of barium (Fig. 7B) and simultaneous depletion of zirconium (less pronounced, Fig. 7F), yttrium (Fig. 7H), nickel (Fig. 7J) and zinc (Fig. 7L) that forms a thin line parallel to the anode surface which possibly signifies the formation of crack or delamination. Interestingly, the cerium distribution appears to be uniform in this area, as seen in Fig. 7D. Secondly, the substantial depletion of zinc on the anode side of the pellet, as visible in Fig. 7L. Such depletion can be

caused by the reactions between hydrogen and ZnO in the reducing H_2 atmosphere on the anode side and subsequent evaporation at the SLFC's operating temperatures. It is known that even the ZnO faces of the lowest surface energy are etched in hydrogen [49]. During this process, ZnO bonds break by hydrogen adsorption on both O and Zn sites forming hydrides. ZnH and ZnH_2 have been reported to be gaseous hydrides desorbing at the relatively low temperature of 380 K. Moreover, hydrogen adsorbed on the Zn-polar surface is so reactive that it is capable of reducing ZnO to metallic Zn, which melts at 692 K and may easily evaporate. This result indicates that a semiconductor that does not contain Zn would be required. Another potentially interesting approach would be replacing LNZ, not with a different mixture of semiconducting oxides, but a material of an entirely different class, for example, one of the so-called triple-conducting oxides (H^+, O^{2-}, e^-) used as novel cathodes in proton conducting fuel cells [51,52].

4. Conclusions

A proton-conducting single layer fuel cell based on the dense composite of $BaCe_{0.6}Zr_{0.2}Y_{0.2}O_{3-\delta}$ and Li_2O:NiO:ZnO (LNZ) semiconducting oxides was presented.

The OCV of the cell was stable and between 0.78 V and 0.83 V in the temperature range of 400–600 °C. An interesting correlation between temperature dependencies of OCV and ohmic ASR was observed and discussed. The obtained power density was low. It reached the value of 3.86 mW cm^{-2} at 600 °C. It was proposed that high polarization resistances and low power density are caused by insufficient porosity and uneven distribution of semiconducting phase in the

composite. A possible solution is to establish the optimal microstructure and porosity, simultaneously low enough to prevent internal combustion and sufficiently high to increase efficiency and power output.

Both the observed formation of a solid solution between NiO and ZnO in as-sintered samples, as well as the zinc redistribution after continued operation in fuel cell conditions are major issues with the LNZ oxides. Either the composition of the semiconducting phase needs adjustment, or an entirely different type of material should be used to provide sufficient electronic conductivity to obtain a reliable single layer fuel cell. Both approaches have their merits and are worth investigating.

Further research, especially systematic studies that aim to establish and explain the underlying principles and working mechanism of single layer fuel cells are required to achieve proton-conducting SLFCs that will match the performance of state-of-the-art solid oxide fuel cells.

Acknowledgements
This work was supported by the National Science Centre, Poland [grant number 2015/19/N/ST5/02639].

References

[1] J.O. Bockris, A Hydrogen Economy, Science (80-.). 176 (1972) 1323–1323. doi:10.1126/science.176.4041.1323.

[2] N.H. Behling, Chapter 2 – Fuel Cells and the Challenges Ahead, in: Fuel Cells, 2013: pp. 7–36. doi:10.1016/B978-0-444-56325-5.00002-8.

[3] A. Lajunen, T. Lipman, Lifecycle cost assessment and carbon dioxide emissions of diesel, natural gas, hybrid electric, fuel cell hybrid and electric transit buses, Energy. 106 (2016) 329–342. doi:10.1016/j.energy.2016.03.075.

[4] J. Lewis, Stationary fuel cells – Insights into commercialisation, Int. J. Hydrogen Energy. 39 (2014) 21896–21901. doi:10.1016/j.ijhydene.2014.05.177.

[5] O.Z. Sharaf, M.F. Orhan, An overview of fuel cell technology: Fundamentals and applications, Renew. Sustain. Energy Rev. 32 (2014) 810–853. doi:10.1016/j.rser.2014.01.012.

[6] J. Wang, Barriers of scaling-up fuel cells: Cost, durability and reliability, Energy. 80 (2015) 509–521. doi:10.1016/j.energy.2014.12.007.

[7] H. Tu, U. Stimming, Advances, aging mechanisms and lifetime in solid-oxide fuel cells, J. Power Sources. 127 (2004) 284–293. doi:10.1016/j.jpowsour.2003.09.025.

[8] H. Yokokawa, H. Tu, B. Iwanschitz, A. Mai, Fundamental mechanisms limiting solid oxide fuel cell durability, J. Power Sources. 182 (2008) 400–412. doi:10.1016/j.jpowsour.2008.02.016.

[9] F. Giannici, G. Canu, M. Gambino, A. Longo, M. Salomé, M. Viviani, et al., Electrode–Electrolyte Compatibility in Solid-Oxide Fuel Cells: Investigation of the LSM–LNC Interface with X-ray Microspectroscopy, Chem. Mater. 27 (2015) 2763–2766. doi:10.1021/acs.chemmater.5b00142.

[10] J. Lyagaeva, D. Medvedev, E. Pikalova, S. Plaksin, A. Brouzgou, A. Demin, et al., A detailed analysis of thermal and chemical compatibility of cathode materials suitable for BaCe0.8Y0.2O3−δ and BaZr0.8Y0.2O3−δ proton electrolytes for solid oxide fuel cell application, Int. J. Hydrogen Energy. 42 (2017) 1715–1723. doi:10.1016/j.ijhydene.2016.07.248.

[11] S. Molin, A. Chrzan, J. Karczewski, D. Szymczewska, P. Jasinski, THE ROLE OF THIN FUNCTIONAL LAYERS IN SOLID OXIDE FUEL CELLS, Electrochim. Acta. 204 (2016) 136–145. doi:10.1016/j.electacta.2016.04.075.

[12] A. Chrzan, J. Karczewski, M. Gazda, D. Szymczewska, P. Jasinski, Investigation of thin perovskite layers between cathode and doped ceria used as buffer layer in solid oxide fuel cells, J. Solid State Electrochem. 19 (2015) 1807–1815. doi:10.1007/s10008-015-2815-x.

[13] H.P. He, X.J. Huang, L.Q. Chen, A practice of single layer solid oxide fuel cell, Ionics (Kiel). 6 (2000) 64–69. doi:10.1007/BF02375548.

[14] H. He, Sr-doped LaInO3 and its possible application in a single layer SOFC, Solid State Ionics. 130 (2000) 183–193. doi:10.1016/S0167-2738(00)00666-4.

[15] B. Zhu, Y. Ma, X. Wang, R. Raza, H. Qin, L. Fan, A fuel cell with a single component functioning simultaneously as the electrodes and electrolyte, Electrochem. Commun. 13 (2011) 225–227. doi:10.1016/j.elecom.2010.12.019.

[16] B. Zhu, R. Raza, G. Abbas, M. Singh, An Electrolyte-Free Fuel Cell Constructed from One Homogenous Layer with Mixed Conductivity, Adv. Funct. Mater. 21 (2011) 2465–2469. doi:10.1002/adfm.201002471.

[17] B. Zhu, R. Raza, Q. Liu, H. Qin, Z. Zhu, L. Fan, et al., A new energy conversion technology joining electrochemical and physical principles, RSC Adv. 2 (2012) 5066. doi:10.1039/c2ra01234k.

[18] Q. Liu, H. Qin, R. Raza, L. Fan, Y. Li, B. Zhu, Advanced electrolyte-free fuel cells based on functional nanocomposites of a single porous component: analysis, modeling and validation, RSC Adv. 2 (2012) 8036. doi:10.1039/c2ra20694c.

[19] K. Zagórski, T. Miruszewski, D. Szymczewska, P. Jasinski, M. Gazda, Synthesis and Testing of BCZY/LNZ Mixed Proton–electron Conducting Composites for Fuel Cell Applications, Procedia Eng. 98 (2014) 121–128. doi:10.1016/j.proeng.2014.12.498.

[20] X. Dong, L. Tian, J. Li, Y. Zhao, Y. Tian, Y. Li, Single layer fuel cell based on a composite of Ce0.8Sm0.2O2−δ–Na2CO3 and a mixed ionic and electronic conductor Sr2Fe1.5Mo0.5O6−δ, J. Power Sources. 249 (2014) 270–276. doi:10.1016/j.jpowsour.2013.10.045.

[21] H. Hu, Q. Lin, Z. Zhu, B. Zhu, X. Liu, Fabrication of electrolyte-free fuel cell with Mg0.4Zn0.6O/Ce0.8Sm0.2O2−δ–Li0.3Ni0.6Cu0.07Sr0.03O2−δ layer, J. Power Sources. 248 (2014) 577–581. doi:10.1016/j.jpowsour.2013.09.095.

[22] L. Fan, C. Wang, O. Osamudiamen, R. Raza, M. Singh, B. Zhu, Mixed ion and electron conductive composites for single component fuel cells: I. Effects of composition and pellet thickness, J. Power Sources. 217 (2012) 164–169. doi:10.1016/j.jpowsour.2012.05.045.

[23] H. Hu, Q. Lin, A. Muhammad, B. Zhu, Electrochemical study of lithiated transition metal oxide composite for single layer fuel cell, J. Power Sources. 286 (2015) 388–393. doi:10.1016/j.jpowsour.2015.03.187.

[24] Y. Lu, B. Zhu, Y. Cai, J.-S. Kim, B. Wang, J. Wang, et al., Progress in Electrolyte-Free Fuel Cells, Front. Energy Res. 4 (2016) 1–10. doi:10.3389/fenrg.2016.00017.

[25] A. Ahmed, R. Raza, M.S. Khalid, M. Saleem, F. Alvi, M.S. Javed, et al., Highly efficient composite electrolyte for natural gas fed fuel cell, Int. J. Hydrogen Energy. 41 (2016) 6972–6979. doi:10.1016/j.ijhydene.2016.02.095.

[26] W. Dong, A. Yaqub, N.K. Janjua, R. Raza, M. Afzal, B. Zhu, All in One Multifunctional Perovskite Material for Next Generation SOFC, Electrochim. Acta. 193 (2016) 225–230. doi:10.1016/j.electacta.2016.02.061.

[27] S.M. Haile, Fuel cell materials and components☆☆☆The Golden Jubilee

Issue—Selected topics in Materials Science and Engineering: Past, Present and Future, edited by S. Suresh., Acta Mater. 51 (2003) 5981–6000. doi:10.1016/j.actamat.2003.08.004.

[28] E. Fabbri, D. Pergolesi, E. Traversa, Materials challenges toward proton-conducting oxide fuel cells: a critical review., Chem. Soc. Rev. 39 (2010) 4355–69. doi:10.1039/b902343g.

[29] E. Fabbri, L. Bi, D. Pergolesi, E. Traversa, Towards the next generation of solid oxide fuel cells operating below 600 °c with chemically stable proton-conducting electrolytes., Adv. Mater. 24 (2012) 195–208. doi:10.1002/adma.201103102.

[30] S. Wang, L. Zhang, L. Zhang, K. Brinkman, F. Chen, Two-step sintering of ultrafine-grained barium cerate proton conducting ceramics, Electrochim. Acta. 87 (2013) 194–200. doi:10.1016/j.electacta.2012.09.007.

[31] Y. Xia, X. Liu, Y. Bai, H. Li, X. Deng, X. Niu, et al., Electrical conductivity optimization in electrolyte-free fuel cells by single-component Ce0.8Sm0.2O2-δ–Li0.15Ni0.45Zn0.4 layer, RSC Adv. 2 (2012) 3828. doi:10.1039/c2ra01213h.

[32] K.M. Dunst, J. Karczewski, T. Miruszewski, B. Kusz, M. Gazda, S. Molin, et al., Investigation of functional layers of solid oxide fuel cell anodes for synthetic biogas reforming, Solid State Ionics. 251 (2013) 70–77. doi:10.1016/j.ssi.2013.03.002.

[33] B. Boukamp, A package for impedance/admittance data analysis, Solid State Ionics. 18–19 (1986) 136–140. doi:10.1016/0167-2738(86)90100-1.

[34] H. Kedesdy, A. Drukalsky, X-Ray Diffraction Studies of the Solid State Reaction in the NiO-ZnO System, J. Am. Chem. Soc. 76 (1954) 5941–5946. doi:10.1021/ja01652a013.

[35] M.K. Deore, Effect of NiO Doping on Structural Properties of ZnO, Int. J. Sci. Res. ISSN (Online Index Copernicus Value Impact Factor. 14611 (2013) 2319–7064. www.ijsr.net (accessed October 27, 2016).

[36] M.G. Wardle, J.P. Goss, P.R. Briddon, Theory of Li in ZnO: A limitation for Li-based p -type doping, Phys. Rev. B. 71 (2005) 155205. doi:10.1103/PhysRevB.71.155205.

[37] K. Gdula-Kasica, A. Mielewczyk-Gryn, S. Molin, P. Jasinski, A. Krupa, B. Kusz, et al., Optimization of microstructure and properties of acceptor-doped barium cerate, Solid State Ionics. 225 (2012) 245–249. doi:10.1016/j.ssi.2012.04.022.

[38] G.-B. Jung, T.-J. Huang, C.-L. Chang, Effect of temperature and dopant concentration on the conductivity of samaria-doped ceria electrolyte, J. Solid State Electrochem. 6 (2002) 225–230. doi:10.1007/s100080100238.

[39] K.D. Kreuer, Proton Conducting Oxides, Annu. Rev. Mater. Res. 33 (2003) 333–359. doi:10.1146/annurev.matsci.33.022802.091825.

[40] L. Zhao, W. Tan, Q. Zhong, The chemical stability and conductivity improvement of protonic conductor BaCe0.8 − x Zr x Y0.2O3 − δ, Ionics (Kiel). 19 (2013) 1745–1750. doi:10.1007/s11581-013-0928-8.

[41] P. Sawant, S. Varma, B.N. Wani, S.R. Bharadwaj, Synthesis, stability and conductivity of BaCe0.8−xZrxY0.2O3−δ as electrolyte for proton conducting SOFC, Int. J. Hydrogen Energy. 37 (2012) 3848–3856. doi:10.1016/j.ijhydene.2011.04.106.

[42] I. EG&G Technical Services, Fuel Cell Handbook, Fuel Cell. 7 Edition (2004) 1–352. doi:10.1002/zaac.200300050.

[43] J. Larminie, A. Dicks, Fuel Cell Systems Explained, Wiley, 2003. doi:10.1016/S0378-7753(00)00571-1.

[44] B. Zhu, P. Lund, R. Raza, J. Patakangas, Q.-A. Huang, L. Fan, et al., A new energy conversion technology based on nano-redox and nano-device processes, Nano Energy. 2 (2013) 1179–1185. doi:10.1016/j.nanoen.2013.05.001.

[45] Q. Wang, J.-E. Moser, M. Grätzel, Electrochemical Impedance Spectroscopic Analysis of Dye-Sensitized Solar Cells, J. Phys. Chem. B. 109 (2005) 14945–14953. doi:10.1021/jp052768h.

[46] Y. Lu, B. Zhu, J. Wang, Y. Zhang, J. Li, Hybrid power generation system of solar energy and fuel cells, Int. J. Energy Res. 40 (2016) 717–725. doi:10.1002/er.3474.

[47] L. Chen, M. Yao, C. Xia, Anode substrate with continuous porosity gradient for tubular solid oxide fuel cells, Electrochem. Commun. 38 (2014) 114–116. doi:10.1016/j.elecom.2013.11.009.

[48] J. Guan, Transport properties of BaCe0.95Y0.05O3−α mixed conductors for hydrogen separation, Solid State Ionics. 100 (1997) 45–52. doi:10.1016/S0167-2738(97)00320-2.

[49] G. Bruno, M.M. Giangregorio, G. Malandrino, P. Capezzuto, I.L. Fragalà, M. Losurdo, Is There a ZnO Face Stable to Atomic Hydrogen?, Adv. Mater. 21 (2009) 1700–1706. doi:10.1002/adma.200802579.

[50] P. Hovington, V. Timoshevskii, S. Burgess, H. Demers, P. Statham, R. Gauvin, et al., Can we detect Li K X-ray in lithium compounds using energy dispersive spectroscopy?, Scanning. 38 (2016) 571–578. doi:10.1002/sca.21302.

[51] C. Duan, J. Tong, M. Shang, S. Nikodemski, M. Sanders, S. Ricote, et al., Readily processed protonic ceramic fuel cells with high performance at low temperatures, Science (80-.). 349 (2015) 1321–1326.

doi:10.1126/science.aab3987.

[52] J. Kim, S. Sengodan, G. Kwon, D. Ding, J. Shin, M. Liu, et al., Triple-Conducting Layered Perovskites as Cathode Materials for Proton-Conducting Solid Oxide Fuel Cells, ChemSusChem. 7 (2014) 2811–2815. doi:10.1002/cssc.201402351.